



ELSEVIER

Fluid Dynamics Research 29 (2001) 25–46

---

---

**FLUID DYNAMICS  
RESEARCH**

---

---

## Three-dimensional extensions to Jeffery–Hamel flow

Simon R. Stow<sup>1</sup>, Peter W. Duck<sup>\*</sup>, Richard E. Hewitt

*Department of Mathematics, University of Manchester, Oxford Road, Manchester, M13 9PL, UK*

Accepted 8 May 2001

---

### Abstract

We consider two viscous flows, both of which are in a class of three-dimensional flow states that are closely related to the classical Jeffery–Hamel solutions. In the first configuration, we consider a flow between two planes, intersecting at an angle  $\alpha$ , and driven by a line-source-like solution in the neighbourhood of the apex of intersection (just as in classical, two-dimensional, Jeffery–Hamel flow). However, in addition we allow for a flow in the direction of the line of intersection of the planes (in order to capture the broader class of three-dimensional solutions). In this flow, two solution scenarios are possible; the first of these originates as a bifurcation from Jeffery–Hamel flow, whilst the second scenario describes a radial velocity of the classical Jeffery–Hamel form (also with a zero azimuthal velocity component), but with an axial velocity determined from the radial flow. Both of these solutions are exact within the Navier–Stokes framework. In the second configuration, we consider the high Reynolds number, three-dimensional flow in a diverging channel, with (generally) non-straight walls close to a plane of symmetry, and driven by a pressure gradient. Similarity solutions are found, and a connection with Jeffery–Hamel flows is established for the particular case of a flow through straight (but non-parallel) channel walls, and again, additional three-dimensional solutions are found. One member of this general class (corresponding to the flow through a straight-walled channel, driven by linearly increasing pressure in both the axial and cross-channel directions), leads to a further family of exact Navier–Stokes solutions. © 2001 Published by The Japan Society of Fluid Mechanics and Elsevier Science B.V. All rights reserved.

*Keywords:* Jeffery–Hamel; Exact Navier–Stokes solutions; Three-dimensional boundary layers

---

### 1. Introduction

Discussion of the two-dimensional flow of a viscous, incompressible fluid between two plane walls separated by an angle  $2\alpha$  and driven by a line-source at the apex dates back to the work of Jeffery (1915) and Hamel (1916). Writing the radial velocity component,  $u$ , in the form  $MG(\vartheta)/r$ , where  $r$  denotes the radial distance from the source,  $\nu$  the kinematic viscosity of the fluid,  $\vartheta$  is the azimuthal

---

<sup>\*</sup> Corresponding author.

*E-mail addresses:* duck@ma.man.ac.uk (P.W. Duck), hewitt@ma.man.ac.uk (R.E. Hewitt).

<sup>1</sup> Present address: Department of Engineering, University of Cambridge, UK.

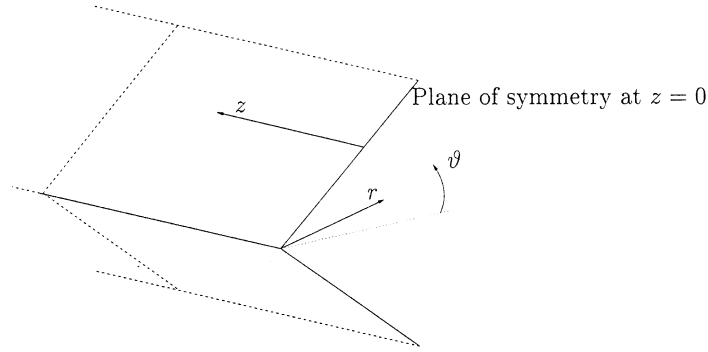


Fig. 1. The geometry and coordinate system for the flow between two inclined planes. There is a line-source-like forcing at the intersection of the two planes, and the flow is assumed to have a plane of symmetry at  $z = 0$ .

angle (the plane walls lying along  $\vartheta = -\alpha$  and  $\alpha$ ) and  $M$  denotes the mass flux between the walls, i.e. (Fig. 1),

$$M = \frac{1}{2} \int_{-\alpha}^{\alpha} u(\vartheta) r \, d\vartheta. \quad (1)$$

This leads to the governing equation,

$$G_{\vartheta\vartheta\vartheta} + 2RGG_{\vartheta} + 4G_{\vartheta} = 0, \quad (2)$$

where the Reynolds number  $R = M/\nu$ . This formulation is exact within the Navier–Stokes framework; the azimuthal velocity component is zero in this case and the no-slip boundary conditions applied at each plane wall reduce to

$$G(-\alpha) = G(\alpha) = 0. \quad (3)$$

It is often more convenient to introduce  $G(\vartheta) = F'(\varphi)/\alpha$ , where  $\varphi = \vartheta/\alpha$ , resulting in

$$F^{(iv)} + 2R\alpha F'F'' + 4\alpha^2 F'' = 0 \quad (4)$$

with boundary conditions  $F(\pm 1) = F'(\pm 1) = 0$  on  $\varphi = \pm 1$ . Thus, we have a fourth-order boundary-value problem, in which the wall angle ( $\alpha$ ) and the net radial mass flux ( $R$ ) can be independently specified and a solution then sought to (4).

The richness of this problem was first fully realized by Rosenhead (1940). There can be an infinity of solutions, depending on the exact choice of apex angle and Reynolds number (i.e., the mass flux). A full classification of solutions has been given by Fraenkel (1962); below we give just a brief overview of the more relevant details.

Each solution to this system can be uniquely identified by (for example) a point in the four-dimensional parameter space

$$(\alpha, R, F''(-1), F'''(-1)),$$

however, some insight can be gained by identifying limiting boundaries in the  $(\alpha-R)$  plane. It is clear that starting at some low- $R$  solution and a fixed angle  $\alpha$ , one may continue a solution to  $R > 0$

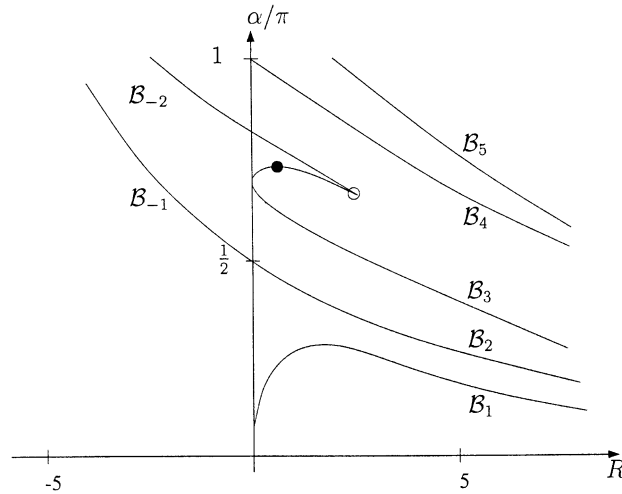


Fig. 2. A schematic of the boundaries in  $\alpha$ - $R$  space along which the Jeffery–Hamel solutions possess special properties (after Fraenkel, 1962 and Banks et al., 1988).

(net out-flow) or  $R < 0$  (net in-flow). In fact, the solutions to (4) can be approached analytically via Jacobian elliptic functions. However, the problem is nonlinear, and non-uniqueness of solutions at fixed wall angle and Reynolds number is common. In this regard one may be interested in those points in the  $(\alpha, R)$  plane that correspond to bifurcations of the Jeffery–Hamel states. These boundaries are shown schematically in Fig. 2, a full description of which is not given here. Nevertheless, some of the properties that the solutions possess on the boundaries presented in Fig. 2 are useful in this work.

The boundary  $\mathcal{B}_1$  and the  $R$ -axis enclose a region in which solutions of type  $I, II_1$  are available (as denoted by Fraenkel, 1962); these states correspond to a symmetric flow with a single velocity maximum, and no reverse flow. The most significant reverse flow solution is denoted by  $II_2$ , which exists between boundaries  $\mathcal{B}_2$  and  $\mathcal{B}_1$ . These states are symmetric about the mid-plane with a single maximum and a reverse-flow region near each wall.

The boundaries  $\mathcal{B}_2$  and  $\mathcal{B}_{-1}$  correspond to a pitchfork bifurcation leading to a further pair of states related by the transformation  $\vartheta \rightarrow -\vartheta$ . The bifurcation is straightforward to describe (see Banks et al., 1988); since the equation is invariant under rotations, given any solution  $G(\vartheta)$ , we can construct a further solution in the form  $G(\vartheta + \delta\vartheta) = G_1(\vartheta) + \delta G'(\vartheta) + \dots$ , therefore a bifurcated state that loses the mid-plane symmetry can be constructed for those symmetric Jeffery–Hamel flows that satisfy  $G'(0) = 0$ . It is this property that is possessed by the states along the boundary  $\mathcal{B}_2$ . We note that this boundary corresponds to solutions for which  $R = 0$  (no net radial mass flux) when  $\alpha = \pi/2$ .

The boundaries  $\mathcal{B}_3$  and  $\mathcal{B}_{-2}$  denote a fold in the solution surface beyond which a sub-set of solutions cannot be continued. The point marked by the open circle in Fig. 2 is a cusp and is formed by the projection of the tangent planes of the fold onto the  $(\alpha, R)$  plane. Obviously, this feature is simply a pitchfork bifurcation unfolded under two control parameters (see, for example, Benjamin, 1978). The point denoted by the filled circle in Fig. 2 corresponds to a transcritical

bifurcation found at  $\alpha = \mu_1\pi$ , where  $\mu_1 \approx 0.74135$ . As we shall show, this latter point is of some significance in the development of three-dimensional states.

In this paper we consider two classes of flow, both of which may be regarded as three-dimensional counterparts (or otherwise closely related) to classical Jeffery–Hamel flows. In Section 2, we consider the flow in the sector formed by two intersecting planes, akin to the Jeffery–Hamel problem, but in addition to the radial flow, we also allow a crossflow which increases linearly in magnitude in the direction of the line of intersection of the two planes. Two distinct scenarios appear to be possible in this case. In the first (Section 2.1), three-dimensional solutions bifurcate from one of the classical Jeffery–Hamel solutions at a critical wall angle and radial mass flux. In the second (Section 2.2) the flow in the radial direction is a Jeffery–Hamel flow, but with an associated flow in the direction of the line of intersection of the two planes. Both of these solutions are exact within the Navier–Stokes framework. In Section 3, we consider the flow down a diverging channel, close to a line of symmetry (perpendicular to the channel walls); in this case a pressure gradient drives the fluid motion. In general, these flows involve a high Reynolds number/boundary-layer approximation, but in the special case of straight diverging channel walls, the flow may be regarded as a further three-dimensional extension to Jeffery–Hamel flow; indeed, one set of solutions in this case corresponds to Jeffery–Hamel flow in the limit of zero corner angle. Both symmetric and asymmetric three-dimensional solutions (with respect to the plane midway between the channel walls) are found. Finally, our conclusions are given in Section 4.

## 2. Flow between intersecting planes

Consider a cylindrical-polar coordinate system  $(r, \vartheta, z)$ , centred on two intersecting, semi-infinite planes inclined at an angle  $\alpha$  to each other, with a plane of symmetry for the flow at  $z=0$ ; the geometry of the flow is shown in Fig. 1. In this coordinate system,  $r$  denotes the (radial) distance to the corner apex formed by the intersection of the planes and  $\vartheta$  denotes the corresponding polar angle (the planar walls lying along  $\vartheta = -\alpha$  and  $\alpha$ ). We denote the corresponding velocity components as  $(u, v, w)$  and the pressure as  $p$ ; with  $\rho$  and  $\nu$  taken to be the constant density and kinematic viscosity of the fluid, respectively. We can define a Reynolds number, as before, using  $R = M/\nu$ , where  $M$  is the radial mass transport.

Below we consider two distinct scenarios to this flow, both of which are exact within the Navier–Stokes framework, and both of which have connections with Jeffery–Hamel flow.

### 2.1. The case of linearly increasing crossflow

The first case we consider is that in which the  $w$  velocity component grows linearly in the crossflow ( $z$ ) direction. ‘Sensible’ balancing of terms then determines the radial dependency of the other terms, specifically yielding

$$u = \nu U(\vartheta)/r, \tag{5a}$$

$$v = \nu V(\vartheta)/r, \tag{5b}$$

$$w = 2\nu z W(\vartheta)/r^2, \tag{5c}$$

which upon substitution into the Navier–Stokes equations leads to the following:

$$V_{\vartheta} + 2W = 0, \quad (6a)$$

$$W_{\vartheta\vartheta} + 4W = 2W^2 - 2UW + VW_{\vartheta}, \quad (6b)$$

$$U_{\vartheta\vartheta\vartheta} + 4U_{\vartheta} = U_{\vartheta}V_{\vartheta} - 2UU_{\vartheta} + VU_{\vartheta\vartheta}, \quad (6c)$$

$$V_{\vartheta\vartheta\vartheta} + 4V_{\vartheta} = -V_{\vartheta}V_{\vartheta} - 2UV_{\vartheta} + VV_{\vartheta\vartheta}. \quad (6d)$$

The corresponding boundary conditions are

$$W(-\alpha) = V(-\alpha) = U(-\alpha) = 0, \quad W(\alpha) = V(\alpha) = U(\alpha) = 0. \quad (6e)$$

We note from the form of this governing system that, unlike the classical Jeffery–Hamel flow, the radial mass flux across a surface of fixed  $r$  cannot be specified arbitrarily. Eqs. (6) can be shown to form a sixth-order system with six boundary conditions. One might view this class of exact solution as a special case of a more generally applicable (but not necessarily self-similar) solution. It is for this reason that we choose to nondimensionalize using the kinematic viscosity in (5) rather than the mass flux which is unknown a priori.

From Eq. (6a) together with (6e), we see that we must have  $\int_{-\alpha}^{\alpha} W \, d\vartheta = 0$ , and therefore there is no net mass flux in the  $z$  direction.

As it stands, system (6) is exact; it is possible to extend this form somewhat, for example with the inclusion of additional terms, including other inverse powers of  $r$ , representing a  $r \gg 1$  expansion. However, the exactness of the formulation is lost in such approaches, although it is still possible to develop forms consistent with a high Reynolds number theory.

We note that, if  $W \equiv V \equiv 0$ , then (5) represents Jeffery–Hamel flow since we simply have a two-dimensional flow along a channel with non-parallel, straight walls, and this is confirmed by writing  $U = G$  to obtain (2).

System (6) was solved using a fourth-order Runge–Kutta method (independent checks on the accuracy of the scheme were made using the continuation package AUTO) over the interval  $\vartheta = -\alpha$  to  $\alpha$  (or 0 for the calculation of symmetric states), although for  $W \neq 0$ , all numerical solutions were found to be symmetric about  $\vartheta = 0$ .

The behaviour of the first four solution branches for varying  $\alpha$  is shown in Fig. 3. The branch 2 solution shown in the figure has four sign changes in the profile of  $W$ , while branches 3 and 4 have six and eight sign changes, respectively; for comparison the primary (branch 1) solution has just two sign changes in the profile of  $W$  and is shown as a solid line. It seems from these results that for any even number of sign changes there are an infinite number of solutions, each with progressively larger values of  $|W_{\vartheta}(-\alpha)|$ . The derivatives of the variables at the wall are in general very large (see Fig. 3), but the results were carefully checked both by varying the spatial step-size in the numerical method and by comparing the results with calculations performed using AUTO. These derivatives become much larger still for even higher-order solutions, suggesting that any numerical technique used in their calculation would require high resolution. In Fig. 4, we show profiles of the primary solution branch at a wall angle of  $\alpha = \pi/4$ . This indicates that the radial flow is non-unidirectional, and is (as indeed were all solutions found of this type) symmetrical with respect to  $\vartheta = 0$ ; the same remarks may be made concerning the crossflow, and so by implication the azimuthal velocity component is antisymmetric about this line.

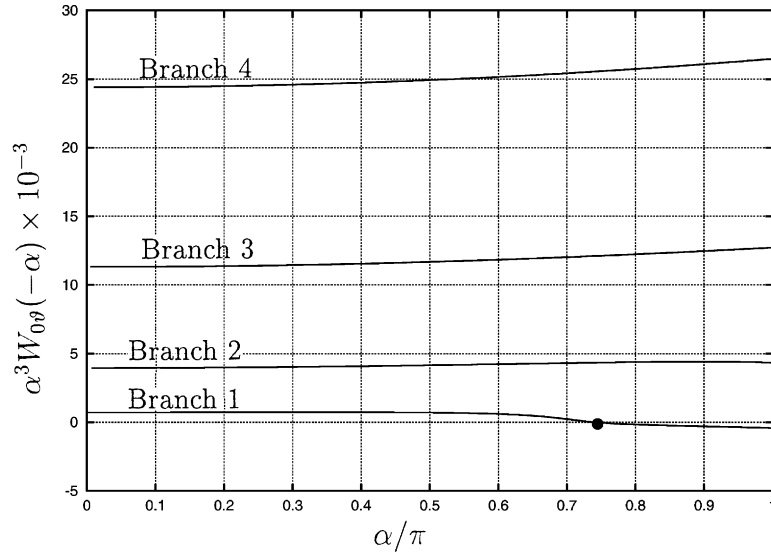


Fig. 3. Variation of  $\alpha^3 W_{0\vartheta}(-\alpha)$  with  $\alpha$  for the first four three-dimensional solution branches. The filled circle denotes the bifurcation of the primary branch from a classical Jeffery–Hamel solution for which  $W \equiv 0$ .

These solutions can be viewed as three-dimensional counterparts of the Jeffery–Hamel solutions with the primary solution branch arising from a bifurcation of one of the Jeffery–Hamel states at a critical wall angle and radial mass flux, as described below.

2.1.1. A bifurcation from Jeffery–Hamel flow

It is easy to show that the governing equations can be rewritten in the form

$$\mathcal{N}_+\{U\} = 0, \tag{7a}$$

$$\mathcal{N}_-\{V\} = 0, \tag{7b}$$

$$W = -DV/2, \tag{7c}$$

where  $\mathcal{N}_\pm$  is the operator

$$\mathcal{N}_\pm \equiv D^3 + 4D + 2UD + VD^2 \pm V'D, \tag{7d}$$

with  $D \equiv d/d\vartheta$ . The boundary conditions are simply

$$U = DV = V = 0, \quad \text{on } \vartheta = \pm \alpha. \tag{7e}$$

We may transform the system further by introducing

$$U = RF'(\varphi)/\alpha, \quad V = H(\varphi)/\alpha, \tag{8a}$$

$$\varphi = \vartheta/\alpha. \tag{8b}$$

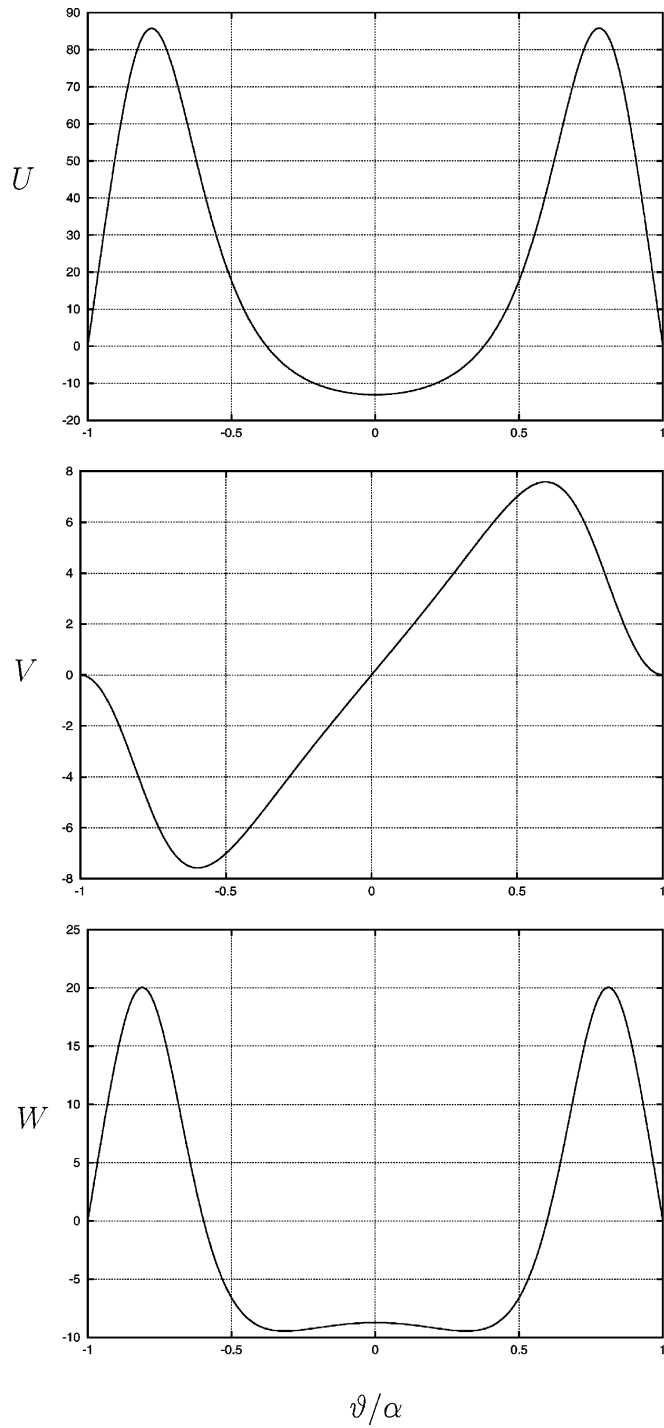


Fig. 4. Profiles of  $U$ ,  $V$  and  $W$  for the primary solution located at  $\alpha = \pi/4$ .

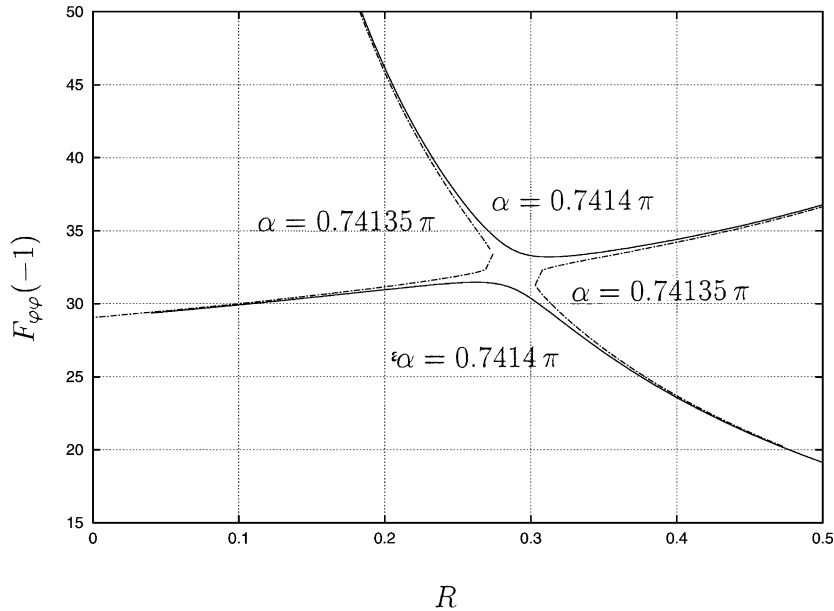


Fig. 5. The Jeffery–Hamel solution branches near the transcritical bifurcation at  $\alpha = \mu_1\pi$ .

Here,  $F'$  is related to the radial velocity component, while  $H$  is associated with the azimuthal velocity and the axial flow is proportional to  $H'$ . The governing system is therefore

$$F^{(iv)} + 2R\alpha F'F'' + 4\alpha^2 F'' - HF''' - H'F'' = 0, \quad (9a)$$

$$H''' + 2R\alpha F'H' + 4\alpha^2 H' - HH'' + H'H' = 0, \quad (9b)$$

where  $F(\pm 1) = \pm 1$ ,  $F'(\pm 1) = H(\pm 1) = H'(\pm 1) = 0$ . Again, here the Reynolds number is  $R = M/\nu$ , where  $M$  is the radial mass flux.

We note that if there is no axial component of velocity,  $H = 0$ , then the equations reduce to those discussed by Fraenkel (1962) and Banks et al. (1988) (and as given by (4)). In this case we obtain a fourth-order equation for  $F(\varphi)$ , with four boundary conditions, and the wall angle ( $\alpha$ ) and Reynolds number ( $R$ , which is essentially a measure of radial mass flux) can be specified independently with the solution classified according to Fig. 2. However, one cannot impose a self-similar *axial* flow at arbitrary points in the  $(\alpha-R)$  parameter space. This can be clearly seen from the form of (9), since it effectively corresponds to a nonlinear eigenvalue problem for the Reynolds number given a fixed  $\alpha$ . Nevertheless, we again expect there to be a locus of points in the  $(\alpha-R)$  plane along which these three-dimensional extensions to Jeffery–Hamel flow exist.

As shown in Fig. 2, there is a boundary  $\mathcal{B}_2$  in the  $(\alpha-R)$  plane along which a fold in the classical Jeffery–Hamel solutions exists. Furthermore, there is a point on this boundary denoted by the filled-circle symbol, which indicates the location of a transcritical bifurcation (at  $\alpha = \mu_1\pi$ ,  $R \approx 0.29$ ). It is at this location that the extension to Jeffery–Hamel flow can be derived as a weakly three-dimensional correction to a leading-order flow of Jeffery–Hamel type. In Fig. 5, we show the Jeffery–Hamel solution branches at fixed values of  $\alpha$  in the neighbourhood of the transcritical

bifurcation. As may be expected,  $\alpha \neq \mu_1\pi$  acts as an imperfection leading to the appearance of fold points if  $\alpha - \mu_1\pi < 0$ , and a region exists in which no neighbouring states can be found as the saddle-node points separate.

To describe the appearance of the three-dimensional solution we can introduce an expansion of the form

$$F = F_f(\varphi) + \varepsilon^{1/2}AF_1^*(\varphi) + \varepsilon F_2(\varphi) + \varepsilon^{3/2}F_3(\varphi) + \dots, \quad (10a)$$

$$H = \varepsilon BH_2^*(\varphi) + \varepsilon^{3/2}H_3(\varphi) + \varepsilon^2H_4(\varphi) + \dots, \quad (10b)$$

$$R = R_0 + \varepsilon, \quad (10c)$$

$$\alpha = \alpha_f(R_0) + \varepsilon[\alpha_f'(R_0) + \alpha_1] + \dots. \quad (10d)$$

Here the subscript f at leading order is used to indicate that this state is the solution on the *fold* boundary  $\mathcal{B}_2$ , and the axial flow is of  $O(\varepsilon)$ , which is the perturbation to the mass-flux value,  $R_0$ , determined at the fold. The constants  $A$  and  $B$  are amplitude constants to be determined from the expansion scheme applied near to the bifurcation point. As can be seen from the analysis of Appendix A, this expansion is able to capture the description of the solutions along the boundary  $\mathcal{B}_2$ , the transcritical bifurcation and the appearance of the three-dimensional state.

From the solvability conditions required at third order in the expansion scheme, we determine the amplitude equations

$$B - c_1\alpha_1 - c_2A^2 = 0, \quad (11)$$

$$AB = 0, \quad (12)$$

$$B^2 - c_3\alpha_1B - c_4B = 0. \quad (13)$$

Here, the constants  $c_j$  can be determined in terms of integrals of the functions  $\hat{R}_j$  (see Appendix A) and the adjoints of the homogeneous equations.

One set of possible states in the neighbourhood of the bifurcation are such that

$$B = 0 \quad \text{and} \quad A^2 = \frac{c_1}{c_2}\alpha_1, \quad (14)$$

corresponding to the two classical Jeffery–Hamel solutions near the fold, which can be developed at any value of  $R_0$  with  $\alpha = \alpha_f(R_0)$  and perturbed by any value for  $|\alpha_1|$ , but only in one direction (i.e., such that  $c_1\alpha_1/c_2 > 0$ ).

There is also a weakly *three-dimensional* solution such that

$$A = 0, \quad B = c_1\alpha_1 \quad \text{and} \quad \alpha_1 = \frac{c_4}{c_1 - c_3} \quad (15)$$

and this latter solution only exists as a perturbation about the point at which  $\alpha_f'(R_0) = 0$ , that is, at the transcritical bifurcation of the classical Jeffery–Hamel solutions. Furthermore, we can note that the relationship between  $\alpha_1$  and  $B$  is caused by the inability to independently specify both the semi-wall-angle  $\alpha$  and the radial mass flux,  $R$ , for the three-dimensional solutions; there is no such restriction in the case  $B = 0$ .

We also note that the normal form of the transcritical bifurcation (as shown in Fig. 5) arises when  $B=0$  and  $\alpha_1=0$ , in which case  $A=0$  is the only solution and a further amplitude constant  $A_2$  is introduced at higher order which then satisfies an amplitude equation of the form  $A_2^2 - d_1 A_2 = 0$ . On writing  $\alpha = \alpha_f + \varepsilon^2 \alpha_2 + \dots$  the bifurcation can be made imperfect, resulting in the amplitude equation  $A_2^2 + d_1 A_2 + d_3 \alpha_2 = 0$ , where  $d_j$  are constants. Solutions of the type shown in Fig. 5 are then easily found. Regions with no solutions are obtained since real solutions to the quadratic amplitude equation only exist for a range of  $\alpha_2$ .

## 2.2. The case of no tangential flow

In this case, assuming there to be no flow in the  $\vartheta$  direction leads to the following forms for the flow components

$$u = vG(\vartheta)/r, \quad (16a)$$

$$v = 0, \quad (16b)$$

$$w = vW(\vartheta)/r, \quad (16c)$$

Substitution of these, into the full Navier–Stokes equations indicates these to be satisfied exactly, provided

$$W_{\vartheta\vartheta} = -(U + 1)W, \quad (17a)$$

$$G_{\vartheta\vartheta\vartheta} + 4G_{\vartheta\vartheta} + 2GG_{\vartheta} = 0 \quad (17b)$$

with  $W(\pm\alpha) = G(\pm\alpha) = 0$ . Note that Eq. (17a) is linear in  $W$  and so (unlike in Section 2.1) we may scale  $W$  by any constant and still have an acceptable solution. To remove this arbitrariness we may make a choice of normalization, for example  $\max|W| = 1$ . From (17b) we see that there is a Jeffery–Hamel flow in the radial direction (as can be seen by comparison with Eq. (2)), with an associated flow in the axial direction, but no tangential flow in the crossflow plane (again, in line with classical Jeffery–Hamel flow).

Since the equation for  $W$  is linear and second order with a no-slip condition applied at both walls, solutions of this form essentially provide an eigenvalue problem of the form

$$\mathcal{F}(\alpha, R; G(\vartheta)) = 0. \quad (18)$$

Thus, a superimposed axial flow  $W$  can be obtained only for a subset of the Jeffery–Hamel solutions that satisfy the additional constraint (18).

The points at which the eigenvalue problem (18) can be satisfied can be easily determined numerically. In Fig. 6, we show the values of  $\alpha$  and  $R$  for which a solution to the eigenvalue problem exists. As can be observed, the solution is unique for  $\alpha \leq \pi/2$ , at which point the Jeffery–Hamel solution passes through boundary  $\mathcal{B}_2$  (as discussed by Fraenkel (1962) and illustrated by Fig. 2) the mid-plane symmetry is broken and a further pair of solutions arises. For  $\alpha > \pi/2$  the solutions either have a net radial inflow ( $R < 0$ ) or zero mass flux in the axial direction (as noted in the figure,  $W$  is antisymmetric for those states arising from  $R=0$  at  $\alpha = \pi/2$ ). The filled squares in Fig. 6 indicate the intersection with critical boundaries  $\mathcal{B}_2$  and  $\mathcal{B}_4$  ( $G$  is trivial at both points).

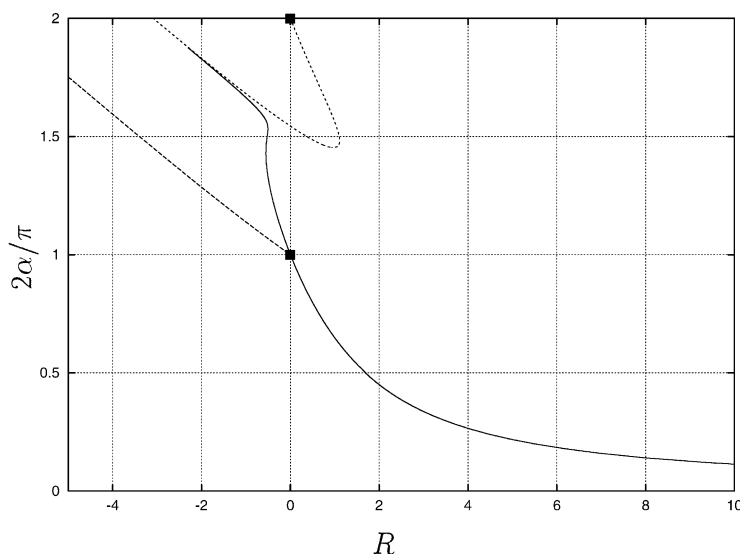


Fig. 6. The points in the  $(\alpha-R)$  plane for which a solution to the eigenvalue problem  $\mathcal{F} = 0$  exists. Note that the appropriate Jeffery–Hamel solution is trivial at the points denoted by the square symbols. Solid line:  $G$  and  $W$  are both symmetric about the mid-plane. Dashed (long) line:  $G$  and  $W$  are both asymmetric about the mid-plane (obviously a pair of states exists at these values). Dashed (short) line:  $G$  is symmetric and  $W$  is antisymmetric about the mid-plane.

It is worth noting that Banks et al. (1988) have suggested that the boundary  $\mathcal{B}_2$  plays a crucial role in divergent channel flows. In particular, on the basis of a ‘spatial stability’ analysis, it was suggested that the inlet and outlet conditions in any finite channel will effect the solution over the entire length when the mass flux exceeds a critical value,  $R_2(\alpha)$ , which is defined as the value at the boundary  $\mathcal{B}_2$ .

To conclude this section, it is perhaps worth noting that both the forms of solution studied, namely (5) and (16), can be derived in a quite formal fashion, as performed by Stow (1999).

### 3. Flow in a diverging channel, close to a plane of symmetry

Here we consider a fully three-dimensional class of flow, which is similar in some respects to the work contained in Section 2. The flow configuration we consider is the flow within a diverging channel (as illustrated in Fig. 7), close to a plane of symmetry, taken to lie in  $z = 0$  (note the channel is unbounded as  $z \rightarrow \pm\infty$ ). We assume that the (generally non-straight) walls of the channel lie along  $y = \pm \lambda \text{Re}^{-1/2} x^{(1-n)/2}$ ; it is then useful to define a scaled transverse coordinate  $Y = \text{Re}^{1/2} y$ , such that the channel walls then lie along  $Y = \pm \lambda x^{(1-n)/2}$ . Here, since the flow is forced by a pressure gradient in the  $x$  direction, we define  $\text{Re} = U_\infty L/\nu$ , where  $U_\infty$  is the typical velocity scale, and  $L$  is a typical streamwise scale over which the channel width increases (or over which the pressure changes significantly), both of which are used for non-dimensionalisation purposes.

We suppose the non-dimensionalised velocity components in the  $(x, y, z)$  (non-dimensional) directions are  $(u, v, w)$ , respectively (here the use of Cartesian coordinates is more appropriate). We

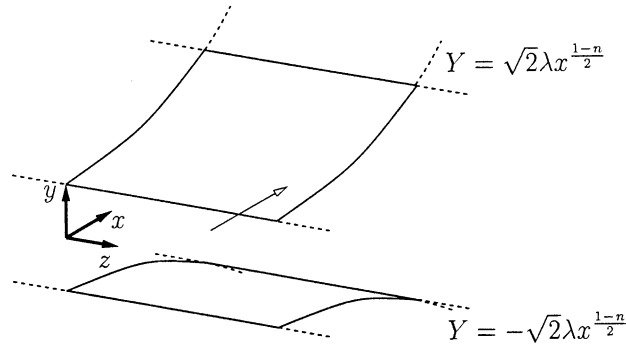


Fig. 7. The geometry for the flow near a plane of symmetry.

now seek similarity solutions to the problem (as  $z \rightarrow 0$  and  $\text{Re} \rightarrow \infty$ ), for which it is necessary to impose an applied pressure (driving the flow) of the form

$$P = x^{2n}\bar{P}_0 + z^2x^{2n-2}\bar{P}_1 + O(z^4) \quad (19)$$

and we shall assume implicitly that  $|z| \ll x$ .

Correspondingly, we seek a (similarity-type) solution of the following form:

$$u = x^n U_0(\eta) + O(z^2), \quad (20a)$$

$$v = \frac{1}{\sqrt{2}} \text{Re}^{-1/2} x^{(n-1)/2} [(1-n)\eta U_0(\eta) - \Phi_0(\eta)] + O(z^2), \quad (20b)$$

$$w = x^{n-1} z W_0(\eta) = \frac{1}{2} x^{n-1} z [(1-n)U_0(\eta) - \Psi_0(\eta)] + O(z^3), \quad (20c)$$

where

$$\eta = Y/x^{(1-n)/2}. \quad (21)$$

This form of solution corresponds to a boundary-layer version (written in a Cartesian form) of that described in Section 2.1. Substitution of this form of solution into the three-dimensional boundary-layer equations (see Dhanak and Duck, 1997), leads to the following leading-order equations:

$$2U_0 = \Phi_{0\eta} + \Psi_0, \quad (22a)$$

$$U_{0\eta\eta} + \bar{P} = 2nU_0^2 - \Phi_0 U_{0\eta}, \quad (22b)$$

$$\Theta_0 = \Psi_{0\eta}, \quad (22c)$$

$$\Theta_{0\eta\eta} - 2(1-n^2)U_0 U_{0\eta} + \Theta_{0\eta} \Phi_0 + \Psi_0 \Theta_0 + 2U_0 \Theta_0 = 0. \quad (22d)$$

The boundary conditions are

$$U_0(\pm\lambda) = \Phi_0(\pm\lambda) = \Psi_0(\pm\lambda) = 0 \quad (22e)$$

and for symmetric flows we also have that

$$U_{0\eta}(0) = \Phi_0(0) = \Theta_0(0) = 0. \quad (22f)$$

In this formulation we have made the substitution  $2n\bar{P}_0 = -\bar{P}$  and note that  $\lambda$  (the domain size) is a parameter of the problem. However, it is more convenient instead to set  $\lambda$  equal to unity and to parameterize the solutions with  $\bar{P}$ ; for consistency, this quantity is independent of  $\eta$ , whilst  $\bar{P}_1$  will vary across the cross section. This can be achieved using the following re-scaling (which is equivalent to changing our definition of  $U_\infty$ ):

$$\eta^{\text{new}} = \lambda^{-1}\eta, \quad \bar{P}^{\text{new}} = \lambda^4\bar{P}, \quad (23a)$$

$$\Phi_0^{\text{new}} = \lambda\Phi_0, \quad U_0^{\text{new}} = \lambda^2U_0, \quad (23b)$$

$$\Psi_0^{\text{new}} = \lambda^2\Psi_0, \quad \Theta_0^{\text{new}} = \lambda^2\Theta_0 \quad (23c)$$

and in our subsequent analysis we shall assume  $\lambda = 1$ .

Two values of  $n$  have particular significance. Firstly, when  $n = 1$  the nozzle has flat, parallel walls (but note that Poiseuille flow is not a solution here because of the assumed form of the pressure gradient which in this case is linear in  $x$ ). For this case the above results are correct even for *finite* Reynolds numbers since the similarity form removes  $\text{Re}$  from the equations, and hence solutions to (22a)–(22d) give exact Navier–Stokes solutions, assuming there to be no  $O(z^4)$  and higher terms in (19). (This is the only value of  $n$  for which this occurs; for all other values we must assume that  $\text{Re} \gg 1$  and that  $|z| \ll x$ ). Secondly, for  $n = -1$  the walls are straight but non-parallel (diverging). Hence, the basic geometry of the problem (if we ignore the  $z$  dependency) is similar to that for Jeffery–Hamel flow although here we assume the pressure is of the form  $x^{-2}$  instead of  $r^{-2}$  (where  $r$  is the distance from  $x = y = 0$ ). However, as the corner angle tends to zero for the Jeffery–Hamel problem,  $r \rightarrow x$  and hence (to leading order) Jeffery–Hamel solutions for this limit are two-dimensional solutions to the present problem (in which case we have that the  $O(z^2)$  and higher terms in (19) are clearly zero). This is confirmed by the fact that if we seek two-dimensional solutions to (22a)–(22d) with  $n = -1$  (by setting  $\Psi_0 \equiv 2U_0$ ,  $\Phi_0 \equiv 0$ ) we obtain equations equivalent to those for the Jeffery–Hamel problem.

### 3.1. Numerical results

Numerical solutions to system (22a)–(22d) were found using a fourth-order Runge–Kutta method, integrating from  $\eta = -1$  to 0 (for symmetric flows) or  $\eta = 1$  (for non-symmetric flows).

#### 3.1.1. The case $n = 0$

Fig. 8 shows the variation of  $U_{0\eta}(-1)$ ,  $\Theta_0(-1)$ ,  $\Theta_{0\eta}(-1)$  and  $W_{0\eta}(-1)$  with  $\bar{P}$  for  $n = 0$ , all the solutions are symmetric. With  $\bar{P} = 0$ , that is, no pressure gradient, we have only the trivial solution  $U_0 \equiv \Phi_0 \equiv \Psi_0 \equiv 0$ . All other solutions have  $W_0 \neq 0$  and hence are inherently three dimensional in nature. For  $\bar{P} > 0$  we have a solution branch emanating from this trivial solution which has a limit point at  $\bar{P} \approx 6.2341$ , after which the branch becomes singular as  $\bar{P} \rightarrow 0_+$ ; the asymptotic form of the solution in this limit is non-trivial and described in Appendix B. For  $\bar{P} < 0$  the solution branch continues from the trivial solution to another limit point at  $\bar{P} \approx -23.534$  and beyond this point the solution becomes singular. For  $\bar{P} > 0$  the solutions represent pure out-flow (i.e.,  $U_0 \geq 0$  for all  $\eta \in [-1, +1]$ ), and pure in-flow for  $\bar{P} < 0$ . This correlation does not hold in general when  $n \neq 0$  as we shall discuss below.

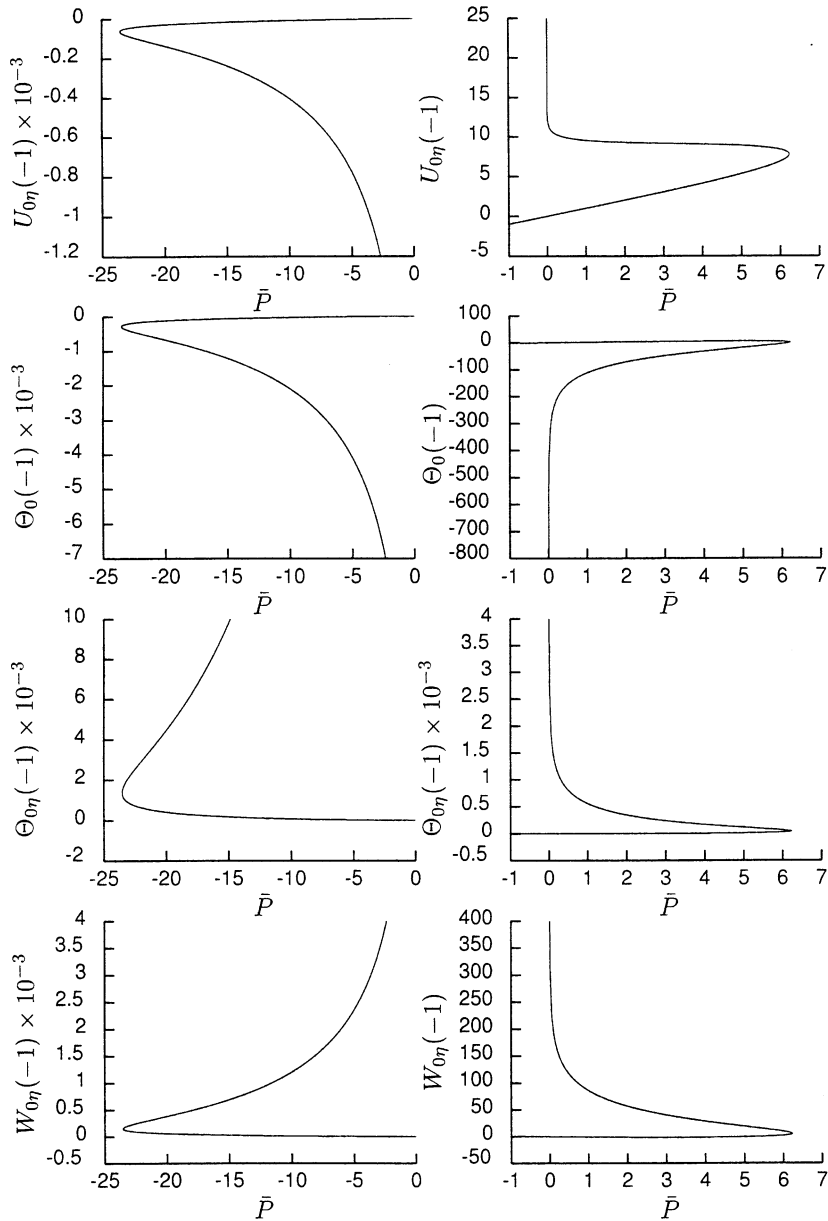


Fig. 8. Variation of  $U_{0\eta}(-1)$ ,  $\Theta_0(-1)$ ,  $\Theta_{0\eta}(-1)$  and  $W_{0\eta}(-1)$  with  $\bar{P}$  for  $n=0$ .

3.1.2. The case  $n=1$ : plane parallel walls

As noted already, in this case our solutions may be regarded as exact within the Navier–Stokes framework. Fig. 9 shows the computed results for  $n=1$ ; all the solutions were found to be symmetric and three dimensional. For large  $\bar{P}$  there is just one solution; this consists of an out-flow near the walls but an in-flow at the centre. As  $\bar{P}$  is decreased,  $U_{0\eta}(-1)$  becomes zero at  $\bar{P} \approx 20.147$ ,

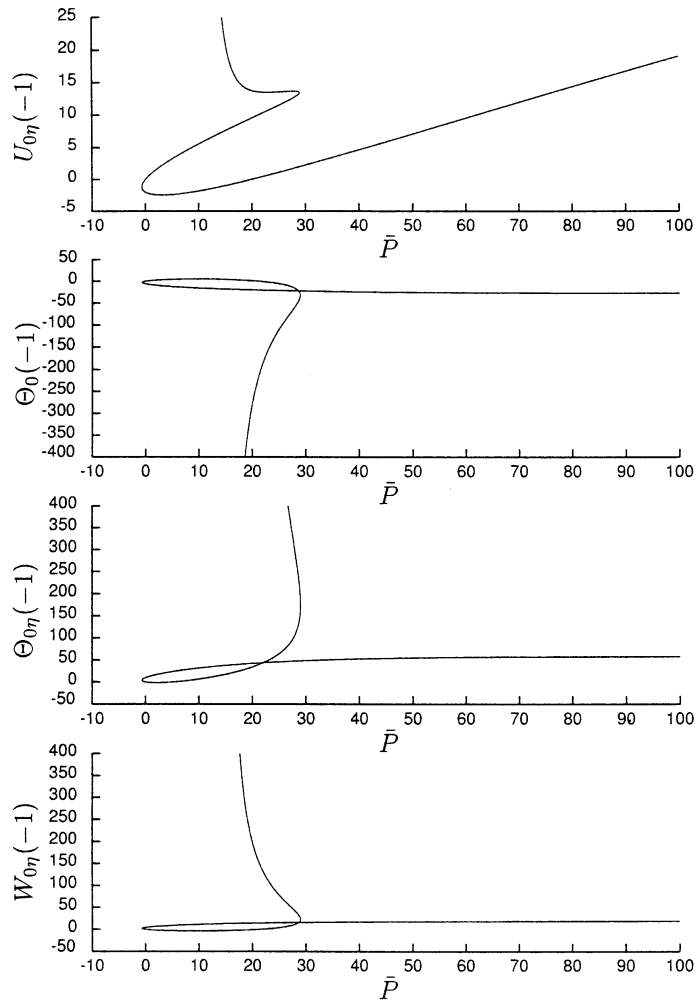


Fig. 9. Variation of  $U_{0\eta}(-1)$ ,  $\Theta_0(-1)$ ,  $\Theta_{0\eta}(-1)$  and  $W_{0\eta}(-1)$  with  $\bar{P}$  for  $n=1$ .

after which the solution consists purely of in-flow, and then the branch passes through a non-trivial solution at  $\bar{P}=0$ . The streamwise flow continues to be directed entirely inwards for all negative  $\bar{P}$ . As  $\bar{P}$  is increased from the trivial state, the solutions indicate a pure out-flow. There is a second limit point, after which the solution becomes singular as  $\bar{P}$  is decreased. The singularity occurs at some value of  $\bar{P} > 0$  (see Appendix B).

### 3.1.3. The case $n = -1$ : Jeffery–Hamel flows

Numerical results for the special case of  $n = -1$  are shown in Fig. 10. This is the only value of  $n$  for which two-dimensional solutions have been located. In the figure, two-dimensional solutions are represented by solid lines for symmetric solutions and short dashes for asymmetric solutions.

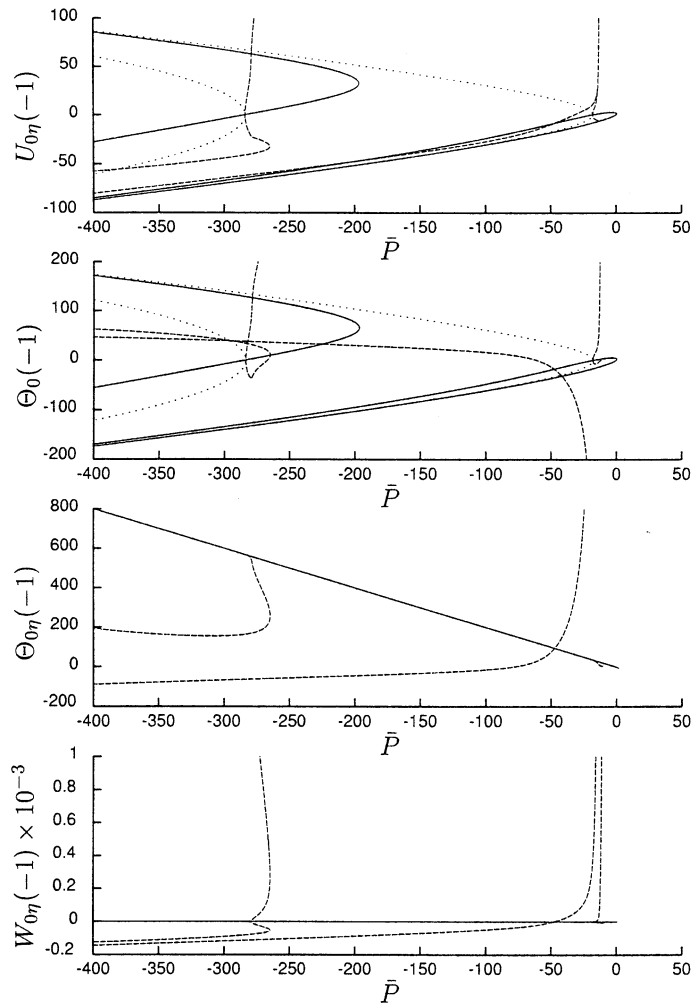


Fig. 10. Variation of  $U_{0\eta}(-1)$ ,  $\Theta_0(-1)$ ,  $\Theta_{0\eta}(-1)$  and  $W_{0\eta}(-1)$  with  $\bar{P}$  for  $n = -1$ .

As stated above these solutions are equivalent to Jeffery–Hamel solutions in the limit of zero corner angle but singular radial mass flux; i.e.,  $\alpha Q = O(1)$  in the notation of Fig. 2.

There are also a number of three-dimensional solution branches present, represented here by long dashes. Firstly, a branch of symmetric solutions was found to bifurcate from the first symmetric, two-dimensional branch when  $\bar{P} \approx -47.438$ . As  $\bar{P}$  is increased this branch becomes singular at a negative value of  $\bar{P}$  (see Appendix B). At  $\bar{P} \approx -31.979$  on this branch  $U_{0\eta}(-1) = 0$ ; for  $\bar{P}$  below this value there is out-flow at the centre with in-flow near the wall, whereas for  $\bar{P}$  above the value there is pure out-flow. Secondly, a branch of asymmetric solutions was found to emanate from two bifurcation points, as shown in the figure. As  $\bar{P}$  increases from the bifurcation point there exists a mirror-image pair of solutions, with  $U_{0\eta}$  soon becoming very large on one wall but not the other.

It is clear from Fig. 10 that there are three bifurcation points, at which three-dimensional states arise from the classical two-dimensional Jeffery–Hamel solutions. The bifurcation near  $\bar{P} \approx -47.438$  is transcritical, with the amplitude of the three-dimensional state developing linearly with a perturbation about the critical pressure gradient. We do not derive the normal form of the bifurcation since it is straightforward and proceeds in a manner analogous to the more complicated case described in Appendix A. The other two points shown in Fig. 10 (near  $\bar{P} \approx -283.609, -17.725$  are both pitchfork bifurcations. As can be observed from the figure, the bifurcations occur at critical values of  $\hat{P}$  that correspond to the appearance of asymmetric states to the two-dimensional Jeffery–Hamel problem; i.e., in the neighbourhood of these bifurcation points there exist symmetric two-dimensional states as well as weakly *asymmetric* two-dimensional and weakly *three-dimensional* states. This behaviour is clearly seen in the asymptotic description of the critical points. Given a perturbation of the form  $\bar{P} = \bar{P}_0 + \varepsilon$  we can introduce the usual description of the pitchfork bifurcation in the form:

$$U_0 = U_{00} + \varepsilon^{1/2}(AU_{01} + BU_{01}^*) + \dots, \quad (24)$$

$$\Psi_0 = 2U_{00} + \varepsilon^{1/2}(2AU_{01} + B\Psi_{01}^*) \dots, \quad (25)$$

$$\Phi_0 = o(\varepsilon^{1/2}). \quad (26)$$

In this expansion  $A$  denotes the amplitude of the asymmetric two-dimensional Jeffery–Hamel state,  $B$  denotes the amplitude of the three-dimensional state, and  $A = B = 0$  corresponds to a symmetric solution of Jeffery–Hamel type. At  $O(\varepsilon^{1/2})$  we obtain eigenvalue problems for  $U_{01}$  and  $(U_{01}^*, \Psi_{01}^*)$ , which act to determine the critical pressure gradient,  $\bar{P}_0$ , at which the bifurcation occurs. It is straightforward to see that the two eigenvalue problems at  $O(\varepsilon^{1/2})$  are identical and therefore in the neighbourhood of these points both two-dimensional asymmetric ( $A \neq 0$ ) and three-dimensional states ( $B \neq 0$ ) can be found. As in Appendix A, we can continue the above expansion to higher order to find the normal form of the pitchfork bifurcation arises through solvability conditions at  $O(\varepsilon^{3/2})$ ; we do not present the details of the derivation here.

### 3.1.4. The case $\bar{P} = 0$ : zero pressure gradient

Figs. 9 and 10 both indicate non-trivial solutions for  $\bar{P} = 0$ . For such solutions there is no pressure gradient so that the flow is being driven totally by its own momentum, in the same way as a jet-flow. In Fig. 11, we trace these solutions as  $n$  is varied. We see that the solutions at  $n = 1$  and  $-1$  are part of separate solution branches. For one branch,  $n$  is always positive and the solutions represent pure in-flow, whereas for the other branch  $n$  is negative and the solutions consist of pure out-flow. Both branches become singular as  $n \rightarrow 0$ ; we do not describe the singularity here, however, details of the asymptotic description can be found in Stow (1999).

## 4. Conclusions

The non-uniqueness of the Jeffery–Hamel class of two-dimension solutions is now well known, and over the years its solution richness has been thoroughly examined, including in more recent times using ideas based on bifurcation theory (Sobey and Drazin, 1986). The results in this paper add yet another dimension to the problem, and indicate that the inclusion of three-dimensionality

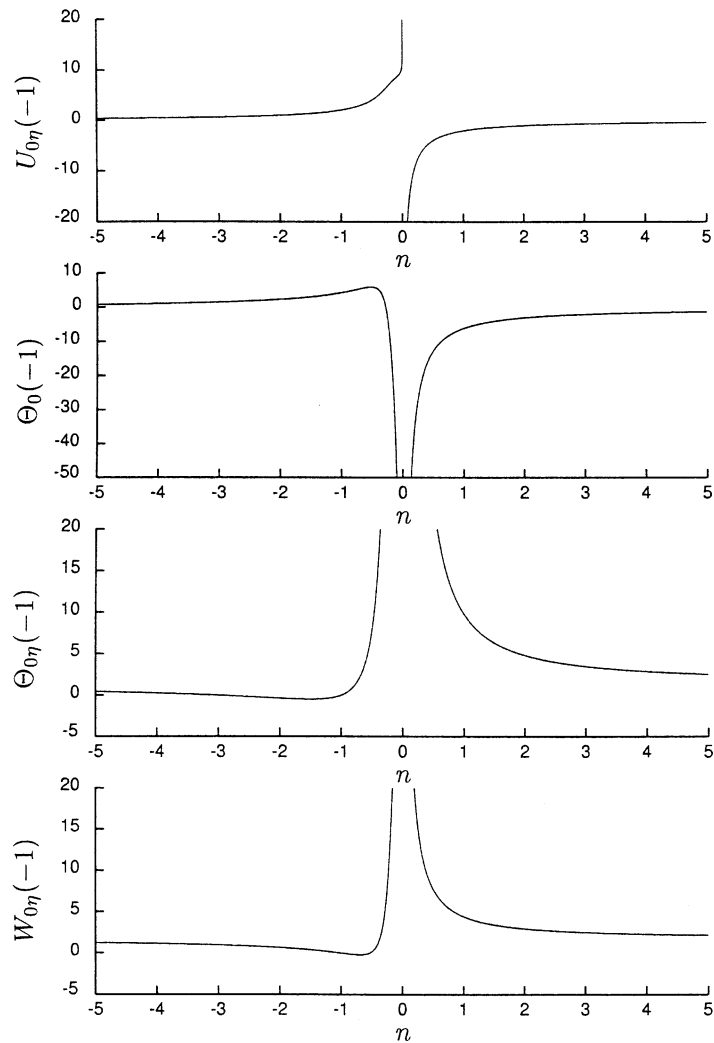


Fig. 11. Variation of  $U_{0\eta}(-1)$ ,  $\Theta_0(-1)$ ,  $\Theta_{0\eta}(-1)$  and  $W_{0\eta}(-1)$  with  $n$  for  $\bar{P}=0$ .

permits a further broadening of flows of this class. The exactness of the formulation, within the framework of the Navier–Stokes equations is generally retained. The natural question to ask is which of the various states is the most realisable, physically. Certainly, there have been a number of serious attempts to answer this for the classical (two-dimensional) case, using arguments based on stability theory. The difficulty of this approach, as highlighted by McAlpine and Drazin (1998), is that it is not possible to separate variables (the procedure normally adopted in Orr–Sommerfeld problems). An allied issue is that of the effect of boundaries on the problem. In the classical case, Dennis et al. (1997) showed that end effects were closely linked to spatial modes. In the present case of three-dimensional variants of the flow, end effects are likely to play a further, even more

complicated role, perhaps even determining solution selection globally; this will form the basis of further investigation.

From a mathematical point of view, these flows are clearly of interest, given their exactness within the Navier–Stokes framework. From a practical point of view such flows are likely to be of some significance in the context (for example) of duct and nozzle flows.

Finally, Professor Philip Drazin has kindly pointed out that form (5) can be generalised to yield a further exact form, merely by considering the flow variables to be a function of  $\vartheta + c \log(r/r_0)$ , rather than just of  $\vartheta$ , where  $c$  and  $r_0$  are constants; this yields a further set of ordinary differential equations, and is currently the focus of our attention.

### Appendix A. Section 2.1 states: a bifurcation from Jeffery–Hamel flow

In the expansion procedure (10a)–(10d), at  $O(\varepsilon^0)$ , we obtain

$$\mathcal{N}_{\text{JH}}\{F_f; \alpha_f, R_0\} = 0, \quad (\text{A.1})$$

where  $\mathcal{N}_{\text{JH}}$  indicates the nonlinear, fourth-order Jeffery–Hamel equation applied with parameters  $\alpha = \alpha_f$  and  $R = R_0$ . The boundary conditions are simply  $F_f(\pm 1) = \pm 1$ ,  $F_f'(\pm 1) = 0$ .

At  $O(\varepsilon^{1/2})$ , we obtain a linear eigenvalue problem for the *fold* location

$$\mathcal{L}_{\text{JH}}\{F_1; \alpha_f, R_0\} = 0. \quad (\text{A.2})$$

Here  $\mathcal{L}_{\text{JH}}$  denotes the operator that arises following linearization of the Jeffery–Hamel equation. This determines the locus of the boundary  $\mathcal{B}_2$ , that is, we determine the functional relationship  $\alpha_f(R_0)$ . The solution at this stage can therefore be written as

$$F_1(\varphi) = AF_1^*(\varphi), \quad (\text{A.3})$$

where  $A$  is an arbitrary (at this stage) amplitude constant.

At next order in the expansion scheme,  $O(\varepsilon)$ , we obtain

$$\mathcal{L}_H\{H_2; \alpha_f, R_0\} = 0, \quad (\text{A.4})$$

where  $\mathcal{L}_H$  is the operator,

$$\mathcal{L}_H \equiv D^3 + 2R_0\alpha_f F_f' D^2 + 4\alpha_f^2 D^2. \quad (\text{A.5})$$

There are four boundary conditions on  $H_2(\varphi)$ , which are  $H_2(\pm 1) = H_2'(\pm 1) = 0$  on  $\varphi = \pm 1$ . We note, however, that (A.4) is both linear and only of third order and therefore we can only satisfy the eigenvalue problem formed by (A.4) by making a particular choice of  $\alpha_f$  and  $R_0$ . In fact, a solution to (A.4) can be constructed from (A.2) by integrating with respect to  $\varphi$  then choosing  $R_0$  such that the constant of integration vanishes. Therefore, a solution to (A.4) exists at the point  $(\alpha_f, R_0)$ , where  $\alpha_f'(R_0) = 0$ , that is, at the transcritical bifurcation of the classical solutions (as marked by the filled circle in Fig. 2). In the neighbourhood of this point in parameter space, a weakly three-dimensional solution can be constructed by the introduction of

$$H_2(\varphi) = BH_2^*(\varphi), \quad (\text{A.6})$$

where again  $B$  is an amplitude constant that remains undetermined at this stage of the expansion.

The equation for  $F_2$  can be simplified at this order by seeking a solution in the form

$$F_2(\varphi) = \frac{dF_f}{dR_0} + \tilde{F}_2(\varphi), \quad (\text{A.7})$$

where

$$\mathcal{L}_H\{\tilde{F}_2; \alpha_f, R_0\} = A^2[2R_0\alpha_f F_1' F_1''] - B[H_2^* F_f'' + H_2^{*'} F_f''] + 2\alpha_1 F_f' F_f''. \quad (\text{A.8})$$

Clearly, for a solution to exist at this order, an orthogonality condition must be satisfied. Nevertheless, we continue to next order before returning to the conditions that determine the amplitude constants. At  $O(\varepsilon^{3/2})$ , we obtain

$$\mathcal{L}_H\{H_3; \alpha_f, R_0\} = ABR_1(\varphi), \quad (\text{A.9})$$

where  $R_1(\varphi)$  is a function that can be given in terms of  $F_1^*$  and  $H_2^*$ . At the following order, we obtain:

$$\mathcal{L}_H\{H_4; \alpha_f, R_0\} = B^2 R_2(\varphi) + \alpha_1 BR_3(\varphi) + BR_4(\varphi), \quad (\text{A.10})$$

where again, the functions  $R_j$  can be given in terms of functions determined at lower order in the expansion.

The amplitude equations (11)–(13) are then determined by deriving the solvability conditions required for solutions to exist to (A.8)–(A.10).

## Appendix B. Asymptotic description of divergent channel flow solutions

We next present asymptotic solutions for certain of the limits described in Section 3.1. For all the limits considered here we find that  $U_{0\eta\eta}(0)$  tends to zero. Furthermore, the limits for which  $U_{0\eta\eta}(0) \rightarrow 0_+$  are all related, as are those for which  $U_{0\eta\eta}(0) \rightarrow 0_-$ .

### B.1. Limit $\bar{P} \rightarrow 0_+$ for $n = 0$

In order to analyse this limit we write  $\varepsilon = \bar{P}$  and consider  $0 < \varepsilon \ll 1$ . To begin with we investigate the region away from both walls and, guided by the above numerical results, we write

$$\Phi_0 = |\log \varepsilon|^a \Phi^*(\eta) + \log |\log \varepsilon| \bar{\Phi}^*(\eta) + \dots, \quad (\text{B.1a})$$

$$U_0 = B + \dots, \quad (\text{B.1b})$$

$$\Psi_0 = |\log \varepsilon|^a \Psi^*(\eta) + \dots, \quad (\text{B.1c})$$

$$\Theta_0 = |\log \varepsilon|^a \Theta^*(\eta) + \dots, \quad (\text{B.1d})$$

where  $a$  and  $b$  are constants, with  $a > 0$ . (The  $\log |\log \varepsilon|$  term in (B.1a) has been included with hindsight, since it appears from the analysis below that this is necessary in order for there to be proper matching with the region near  $\eta = -1$ ). Substituting this expansion into the main system of equations (22a)–(22d) we find that

$$\Psi^* = -\Phi_\eta^*, \quad (\text{B.2a})$$

$$\Theta^* = -\Phi_{\eta\eta}^*, \quad (\text{B.2b})$$

$$\Phi_{\eta\eta}^* \Phi^* - \Phi_\eta^{*,2} = c \quad (\text{B.2c})$$

for some constant  $c$ , the equation for  $U_0$  being treated separately below. A family of solutions to this system is

$$\Phi^* = -A \sin \pi \eta \quad (\text{B.3})$$

with  $A > 0$  (suggested by the profiles of  $\Phi_0$  from numerical solutions).

Full details of the analysis may be found in Stow (1999), but the next important point is the existence of a region near  $\eta = -1$ , of thickness  $O(|\log \varepsilon|^{-a/2})$ , which when matched with the  $\eta + 1 = O(1)$  region leads us to the conclusion that

$$a = 1, \quad A = \frac{\pi}{2}. \quad (\text{B.4})$$

A comparison of the above asymptotic results with results obtained numerically is shown in Stow (1999) and indicates good agreement between the two approaches.

Numerical solutions in the limit  $n \rightarrow 0_-$  for  $\bar{P} = 0$  were found to be similar to those for the limit  $\bar{P} \rightarrow 0_+$  with  $n = 0$ , in particular, the value  $U_0(0)$  appears to be tending to the same finite limit (denoted by  $B$  above). Note that in Section B.1,  $U_{0\eta\eta}(0) = -\varepsilon$ , whereas here  $U_{0\eta\eta}(0) \rightarrow 2nB^2$ . In fact, if we write  $n = -(1/2B^2)\varepsilon$ , the (first-order) asymptotic solution above applies here also. To test this connection numerically, the same variables as in above were compared with “ $\varepsilon$ ” where here we take  $\varepsilon = -2nU_0(0)^2$  since  $B$  is not known accurately; the results confirmed the connection between two limits.

### B.2. Limit $\bar{P} \rightarrow 2nB^2$ for fixed (nonzero) $n$

We now consider the singularity found when varying  $\bar{P}$  for  $n = 1$  (see Fig. 9), as well as the singularity that occurs in the three-dimensional symmetric solution branch for  $n = -1$  (see Fig. 10). As stated above, these two singularities occur at finite non-zero values of  $\bar{P}$ . It was found that the numerical solutions for both cases were similar to those in Section B.1, in particular,  $U_0(0)$  tends to the constant  $B$ . Also  $U_{0\eta\eta}(0)$  was found to tend to zero (from below), suggesting a singularity occurs as  $\bar{P} \rightarrow 2nB^2$ . This was also found to be the case for other values of  $n$ , implying that there is a family of singularities for which  $\bar{P} \rightarrow 2nB^2$ . It was found that  $\bar{P}$  tended to this limit from above when  $n > 0$ , and from below when  $n < 0$ . Furthermore, it appears that the asymptotic solution of Section B.1 applies again, with now  $\varepsilon = \bar{P} - 2nU_0(0)^2$ . But the relationship between  $\bar{P}$  and  $\varepsilon$  is not clear from this expression since  $U_0(0)$  varies with  $\bar{P}$ . Although the value of  $B$  is not accurately known,  $\varepsilon$  must tend to zero much faster than  $\bar{P}$  tends to  $2nB^2$ , i.e.,  $\varepsilon = o(\bar{P} - 2nB^2)$ , suggesting that  $\log \varepsilon \sim \bar{P} - 2nB^2$ . Numerical results (presented by Stow, 1999) confirm the accuracy of the above.

**References**

- Banks, W.H.H., Drazin, P.G., Zaturka, M.B., 1988. On perturbations of Jeffery–Hamel flow. *J. Fluid Mech.* 186, 559.
- Benjamin, 1978. Bifurcation phenomena in steady flows of a viscous fluid. I Theory. *Proc. R. Soc. London A*359, 1.
- Dennis, S.C.R., Banks, W.H.H., Drazin, P.G., Zaturka, M.B., 1997. Flow along a diverging channel. *J. Fluid Mech.* 336, 183.
- Dhanak, M.R., Duck, P.W., 1997. The effect of freestream pressure gradient on a corner boundary layer. *Proc. R. Soc. Lond. A* 453, 1793.
- Fraenkel, L.E., 1962. Laminar flow in symmetrical channels with slightly curved walls. I. On the Jeffery–Hamel solutions for flow between plane walls. *Proc. R. Soc. Lond. A* 267, 119.
- Hamel, G., 1916. Spiralformige Bewegungen Zaher Flussigkeiten. *Jahresbericht Deutch. Math. Verein.* 25, 34–60.
- Jeffery, G.B., 1915. The two-dimensional steady motion of a viscous fluid. *Phil. Mag.* (6) 29, 455–465.
- McAlpine, A., Drazin, P.G., 1998. On the spatio-temporal development of small perturbations of Jeffery–Hamel flows. *Fluid Dyn. Res.* 22, 123.
- Rosenhead, L., 1940. The steady two-dimensional radial flow of viscous fluid between two inclined plane walls. *Proc. R. Soc.* 175, 436.
- Sobey, I.J., Drazin, P.G., 1986. Bifurcations of two-dimensional channel flows. *J. Fluid Mech.* 171, 263.
- Stow, S.R., 1999. On a class of three-dimensional boundary-layer flows. Ph.D. Thesis, University of Manchester.